The Journal of Chemical Physics

RESEARCH ARTICLE | AUGUST 06 2025

Spin crossover in metal–organic frameworks: A crystal embedded multi-reference study

I. Popov ; A. Tchougréeff ; E. Besley

J. Chem. Phys. 163, 054117 (2025)
https://doi.org/10.1063/5.0246625

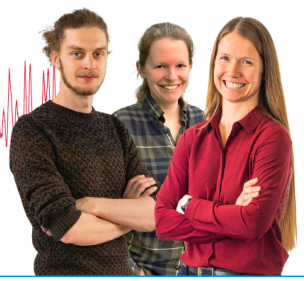

AIP Publishing

The Journal of Chemical Physics ARTICLE pubs.aip.org/aip/jcp

Spin crossover in metal–organic frameworks: A crystal embedded multi-reference study

Cite as: J. Chem. Phys. 163, 054117 (2025); doi: 10.1063/5.0246625
Submitted: 3 November 2024 • Accepted: 14 July 2025 •
Published Online: 6 August 2025

I. Popov,[1] A. Tchougréeff,[2,a)] and E. Besley[1,b)]

AFFILIATIONS

[1] School of Chemistry, University of Nottingham, University Park, Nottingham NG7 2RD, United Kingdom
[2] Frumkin Institute of Physical Chemistry and Electrochemistry Russian Academy of Sciences, Moscow, Russia

[a)] Electronic mail: tchougreeff@phyche.ac.ru
[b)] Author to whom correspondence should be addressed: Elena.Besley@nottingham.ac.uk

ABSTRACT

Spin crossover (SCO) in transition metal (TM)-containing solid state materials remains a challenge for the electronic structure calculations as some of the electronic states may have a significant multi-reference character. The periodic effective Hamiltonian of crystal field (pEHCF) method accurately describes strong correlations in TM-containing crystalline systems. In this work, pEHCF has been applied to study the electronic structure of the high spin and low spin states in the $Fe(pyridine)_2Ni(CN)_4$ metal–organic framework (MOF). The relative energy of the spin states involved in SCO has been calculated, and the degeneracy line exhibiting a strong dependence on the distance between an Fe ion and the CN groups has been identified. The degeneracy line also displays a step-like dependence on the position of the pyridine ligands in the narrow interval of 2.08–2.10 Å, while outside this interval, the dependence is weak. Low-temperature paramagnetism of the $Fe(pyridine)_2Ni(CN)_4$ SCO-MOF has been explained by the triplet ground state of Ni in the square-planar coordination with the CN groups. The electronic structure of a recently synthesized $Fe_2(H_{0.67}bdt)_3$ SCO-MOF has been also investigated. This MOF contains two types of Fe ions and exhibits unusual spin crossover behavior above room temperature. Our calculations confirm that in the temperature range of 300–423 K, Fe_2 ions undergo a spin transition from quintet (S = 2) to singlet (S = 0), while Fe_1 ions exist in the low-spin configuration in both initial (300 K) and final structures (423 K).

I. INTRODUCTION

Rapid proliferation of stimuli-responsive materials brings renewed and growing emphasis on the intricate reversible switching capabilities of transition metal (TM) complexes with energetically close-lying spin states as highly attractive for technological applications in information storage and quantum technologies. A diverse range of molecular complexes, nanoparticles, thin films, and coordination frameworks exhibit spin crossover behavior demonstrated by a change in the spin state of a TM ion triggered by external stimuli such as temperature, pressure, light irradiation,[1,2] magnetic fields, and the adsorption of guest molecules. Metal–organic frameworks displaying spin crossover (SCO-MOFs) exhibit dramatic changes in their physical and chemical properties associated with the spin state change upon external perturbation. This further expands the prospects and capabilities of SCO-MOFs in nanoscale electronic and spintronic devices[1,3–5] and chemical sensing applications.[5–12]

The most common ion used in design of SCO-MOFs is Fe(II) having six electrons in the open *d*-shell. The first iron-containing SCO-MOF, $Fe(pyridine)_2Ni(CN)_4$, was synthesized by Kitazawa *et al.*,[13] which belongs to the class of Hofmann-type MOFs.[14] This material exhibits thermally induced spin crossover in the temperature range of 170–210 K, as evidenced by magnetic susceptibility measurements and ^{57}Fe Mössbauer spectroscopy.[13] In the past 30 years, numerous representatives of the Hofmann-type SCO-MOFs with general formulae $FeL_2M^{II}(CN)_4$ and $FeL_2[M^{I}(CN)_2]_2$ have been prepared and studied in detail[15–25] (here, M^{I} = Ag, Au, M^{II} = Ni, Pd, Pt, and L is an organic ligand, such as pyridine and pyrazine). In addition, various forms of iron-based SCO-MOFs that do not belong to the Hofmann-type frameworks have been described in the literature.[26,27]

The description of electronic and vibrational structure in SCO systems involves many elaborate steps, including calculations of the potential energy surfaces of HS and LS configurations, spin–orbit coupling, and vibronic effects in the vicinity of the degeneracy point. Spin transitions in iron-containing complexes present a particularly challenging case for the electronic structure calculations because the $^1A_1$ state in the octahedral d^6-shell has a significant multi-reference character, while the $^5T_2$ term can be described with a single configuration.[28] For iron containing molecular complexes, the most reliable estimations of the relative energy between the high spin (HS) and low spin (LS) states were obtained with the coupled cluster theory [CCSD(T)] and combined CC/CASPT2 approaches,[29–31] which accurately account for electron correlations in the open *d*-shell. CASPT2 on its own gives a systematic error for spin-crossover complexes of iron (II),[32] but in some cases, the fully internally contracted CASPT2 method demonstrates a reasonably good agreement.[33] When we move from molecular systems to solid-state SCO-MOFs, the application of multi-reference CCSD(T) and CASPT2 methods becomes computationally prohibitive due to the periodic nature of these systems and large unit cell size.

To circumvent these limitations, Kohn–Sham density functional theory (DFT) has been routinely used to study SCO-MOFs.[27,34] With an appropriate selection of the density functional,[35] DFT provides good results for SCO systems; however, significant *d*-shell localization and multi-reference nature of the low-spin state may cause well known problems with accuracy and convergence of DFT when applied to strongly correlated systems, including MOFs with transition metal atoms.[35,36] Hybrid quantum mechanical methods emerge as a viable alternative to computationally expensive multi-reference approaches and DFT. The effective Hamiltonian of crystal field (EHCF) method[37] is an example of a hybrid quantum chemical method, which accurately accounts for electron correlations in open *d*-shells of molecular TM complexes.

In our recent study,[38] we generalized the EHCF method to extended periodic systems containing TM ions with isolated *d*-shells, either as a part of their crystal structure or as point defects. We have also shown[38,39] that for a variety of solid state materials and with modest requirements for computational resources, periodic effective Hamiltonian of crystal field (pEHCF) accurately reproduces the experimental energies of *d*–*d* transitions and spin symmetry of both ground and excited states. The studied materials include metal oxides, carbodiimides, hydrocyanamides, and a series of M-MOF-74 (M = Fe, Co, Ni).[38,39] An additional unique feature of the pEHCF method is the ability to calculate the quadrupole splittings (QS) in ^{57}Fe Mössbauer spectroscopy, which is frequently used in experimental investigations of iron-containing SCO-MOFs.[13,20]

In this work, we extend the pEHCF study to calculate the potential energy surfaces of the high spin and low spin electron configurations of SCO-MOFs in the space of atomic coordinates varying during spin crossover transitions. We demonstrate the viability of the adopted hybrid method on the most thoroughly studied representative of SCO-MOFs, the Hofmann-type $Fe(pyridine)_2Ni(CN)_4$ (**1**) MOF. We further include the study of the electronic structure of a novel non-Hofmann SCO-MOF based on 1,4-benzeneditetrazolate (bdt), $Fe_2(H_{0.67}bdt)_3$ (**2**), which exhibits interesting changes in magnetic properties upon spin transition.[27]

II. METHODOLOGY

The pEHCF method separates the space of one electronic state into two subspaces describing independently the local *d*-shell(s) of transition metal atoms (*d*-subspace) and the crystalline environment embedding the *d*-shell(s) (*l*-subspace spanned by *s, p*-orbitals, where *l* stands for *ligand*).[37,38] All *s, p*-orbitals of TM are included in the *l*-subspace together with the orbitals of light elements. The many-electron wave-function of the system is expressed as

$$\Psi = \Psi_d \wedge \Psi_l, \tag{1}$$

where Ψ_d and Ψ_l are the many-electron wave functions built in the *d* and *l* orbital subspaces and $\wedge$ stands for the anti-symmetric product. All local *d*-shells in the equivalent crystallographic positions are considered to be equal, i.e., to have the same electronic state. This description of the electronic structure of TM-containing insulators was first proposed by Harrison,[40] who suggested that the electronic structure can be viewed as a set of delocalized *sp*-bands augmented by the local *d*-multiplets of individual TM atoms. Following this idea, we express the wave function of the *d*-system as an anti-symmetric product of the wave functions of individual local *d*-shells,

$$\Psi_d = \wedge_{\mathbf{r}} \wedge_{i=1}^{k} \Psi_d^{(i\mathbf{r})}, \tag{2}$$

where **r** goes over all unit cells in the system and index *i* enumerates *d*-shells in the unit cell.

The wave functions Ψ_d and Ψ_l are treated at different levels of theory. For each *d*-shell, the strongly correlated *d*-subspace is described by the full configuration interaction (full CI) method, which takes into account static electron correlations in the *d*-shell and accurately reproduces the energy and spin multiplicity of the excited *d*-multiplets. The wave function of the *l*-system is presented as a single Slater determinant constructed from crystal orbitals expressed as a linear combination of the Bloch sums of atomic orbitals. In principle, the pEHCF methodology allows the use of any method utilizing the one-electron approximation to describe the electronic structure of the *l*-system. In this work, it is calculated using the solid-state semi-empirical CNDO method with the standard parameters for the light elements and Clack's parameters for *s, p*-orbitals of transition atoms.[41]

Taking into account that pEHCF is a hybrid method, the effective Hamiltonian contains specific terms describing interactions of *d*- and *l*-subsystems, as described in our previous works.[38,42] The wave function in (1) assumes fixed number of electrons in the *d*- and *l*-subspaces, thus excluding the states involved in the electron charge transfer. The charge transfer states are taken into account by the Löwdin partitioning technique,[43] which provides effective corrections to the Hamiltonian operators of the two subspaces through the resonance coupling terms.[37] This leads to the following form of the effective Hamiltonian for the *d*-subspace:

$$H_d^{\text{eff}} = \sum_{\mu\nu}\sum_{\sigma}\left(H_{\mu\nu}^{d} + H_{\mu\nu}^{\text{coul}} + H_{\mu\nu}^{\text{res}}\right) d_{\mu\sigma}^{+} d_{\nu\sigma} + \frac{1}{2}\sum_{\mu\nu\lambda\eta}\sum_{\sigma\tau}(\mu\nu|\lambda\eta) d_{\mu\sigma}^{+} d_{\lambda\tau}^{+} d_{\eta\tau} d_{\nu\sigma} + h.c., \tag{3}$$

where $d^{+}_{\mu\sigma}$ ($d_{\mu\sigma}$) are the electron creation (annihilation) operators for the μth d-orbital and σ corresponds to the spin projection. The last term in Eq. (3) describes the two-electron Coulomb interactions inside the d-shell. The one-electron part of the Hamiltonian includes bare Hamiltonian of the d-system (H^{d}) and Coulomb (H^{coul}) and resonance (H^{res}) interactions of d-electrons with electrons and nuclei of the l-subspace. H^{coul} and H^{res} terms determine the splitting of d-orbitals; in the crystal field theory, these are considered as a parameter. In contrast to the crystal field theory, the main contribution to the splitting of d-orbitals in the EHCF method is due to the resonance interactions[37,38] corresponding to the transfer of an electron between the d- and l-subspaces. Here, H^{res} becomes the most important factor in the analysis of variations in the splitting parameters in spin crossover processes. Therefore, we will describe the functional form of the resonance term in more detail. The matrix elements of H^{res} have the following form:[38]

$$H^{\mathrm{res}}_{\mu\nu} = \sum_{a,b} \beta_{\mu a}\beta_{\nu b}\left\{\Re G^{+}_{ab}(-I_d) + \Re G^{-}_{ab}(-A_d)\right\}, \tag{4}$$

where the summation goes over atomic orbitals a and b of the l-subspace, $\beta_{\mu a}$ are the resonance (hopping) integrals between the μth d-orbital and orbital a, and I_d and A_d are the ionization potential and electron affinity of the d-system. The orbital-projected Green's functions $G^{\pm}_{ab}$ of the l-subspace are expressed as

$$G^{+}_{ab}(\varepsilon) = \lim_{\delta\to 0^{+}} \sum_{n,\mathbf{k}} (1 - f_{n\mathbf{k}}) \frac{\langle a|\, n\mathbf{k}\rangle\langle n\mathbf{k}|\, b\rangle}{\varepsilon - \varepsilon_{n\mathbf{k}} + i\delta}, \tag{5}$$

$$G^{-}_{ab}(\varepsilon) = \lim_{\delta\to 0^{+}} \sum_{n,\mathbf{k}} f_{n\mathbf{k}} \frac{\langle a|\, n\mathbf{k}\rangle\langle n\mathbf{k}|\, b\rangle}{\varepsilon - \varepsilon_{n\mathbf{k}} + i\delta}. \tag{6}$$

In Eqs. (5) and (6), $\mathbf{k}$ is a vector in the first Brillouin zone, n enumerates bands of the l-subspace, and $\varepsilon_{n\mathbf{k}}$ and $f_{n\mathbf{k}}$ are the energy and occupation number of the l-bands. Spin variables are omitted for clarity. The resonance term and, hence, the splitting of the d-orbitals depend on three main factors: (i) geometry of the first coordination sphere through the resonance integrals between the local atomic orbitals, $\beta_{\mu a}$; (ii) occupation of the local atomic orbitals forming the first coordination sphere; and (iii) energy difference between the d-states and valence/conduction bands of the l-subsystem.

The quadrupole splittings of the ^{57}Fe Mössbauer spectrum can be calculated from the multiplet structure of the d-shell as described in Ref. 39. In this work, we mostly focus our attention on the lowest lying high spin ($S = 2$) and low spin ($S = 0$) states in the d-shells of iron (II) ions.

III. RESULTS AND DISCUSSION

Figure 1(a) shows the crystalline structure of **1** in which Fe and Ni ions are arranged in the corrugated 2D layers coupled by CN groups so that N atoms coordinate with Fe and C atoms are connected to Ni. Pyridine molecules are axially attached to Fe ions, which have the total coordination number of six. The distance between Fe and the N atoms of CN groups (denoted as N_1) is smaller than the Fe–N_2 distance between Fe and pyridine. This results in a distorted octahedral coordination sphere corresponding to the D_{4h} symmetry [see Fig. 1(b)]. Ni has a square-planar coordination corresponding to the same point group.

The room-temperature (RT) structure[13] of **1** has the distance d(Fe–N_1) = 2.155 Å and d(Fe–N_2) = 2.208 Å, whereas in the low-temperature (LT) structure,[44] d(Fe–N_1) = 1.935 Å and d(Fe–N_2) = 1.985 Å. The results of the pEHCF calculations for these two structures are collected in Tables I and II. In agreement with experiment,[13] the calculated spin of the ground state of Fe ions is $S = 2$ (high-spin) in the RT structure and $S = 0$ (low-spin) in the LT geometry. The calculated values of the ^{57}Fe Mössbauer quadrupole splittings are 3.62 mm/s at room temperature and 1.65 mm/s at low temperatures, which can be compared with the reported experimental difference in the quadrupole splitting of 0.86 mm/s in favor of the RT value.[13] In agreement with experiment, the RT structure is characterized by a higher quadrupole splitting; however, the calculated difference is overestimated by 1.11 mm/s.

Although the LT structure of **1** contains diamagnetic iron (II) ions, it exhibits paramagnetic behavior in experiments.[13,15,45] Mössbauer[45] and temperature-dependent EXAFS[44] studies show that the spin-transition of Fe (II) is complete below 100 K, so the residual paramagnetism of LT had been associated with paramagnetic impurities, such as Fe (III).[13,45] The presence of paramagnetic impurities is additionally supported by the effective magnetic moments in the RT structure that can be extracted from the experimental value of magnetic susceptibility. The reported values of $\chi_m T$, measured for the RT structure, are 3.2,[13] 3.49–3.73,[15] and 3.8 cm^3 K mol^{-1},[45] which yield the effective magnetic moments of 5.06μ_B, 5.28–5.46μ_B, and 5.51μ_B, respectively. All these experimental values are noticeably higher than the theoretical estimation of 4.90μ_B for the magnetic moment of high-spin Fe (II), thus suggesting the existence of other paramagnetic ions. Assuming that the higher effective moment comes solely from Fe (III) impurities, we can express it as

$$\mu^{2}_{\mathrm{eff}} = x\mu^{2}_{\mathrm{Fe}^{3+}} + (1 - x)\mu^{2}_{\mathrm{Fe}^{2+}}, \tag{7}$$

where $\mu_{\mathrm{Fe}^{2+}} = 4.90\mu_B$ and $\mu_{\mathrm{Fe}^{3+}} = 5.92\mu_B$ are the magnetic moments of the respective high-spin Fe ions and x is the percentage of Fe (III), which can be estimated as x = 14%–58% for the experimental values of μ_{eff} extracted from Refs. 13, 15, and 45. In addition, the experimental ratio of the effective magnetic moments in the RT and LT structures, $\mu^{\mathrm{RT}}_{\mathrm{eff}} : \mu^{\mathrm{LT}}_{\mathrm{eff}}$ = 2.15–2.53,[13,15] gives a comparable estimation of the percentage of Fe (III) lying in the range of 15%–20%. Such a concentration of impurities is extremely unlikely in a good quality sample. By contrast, the estimation of the Fe (III) concentration from the Mössbauer spectrum yields ~3% for system **1**,[45] which is also consistent with the elemental analysis reported there.

An alternative source of the higher magnetic moment of system **1** could potentially be Ni (II) ions, which have d^8 configuration and can exist in the triplet state. The ratio of the effective magnetic moments, $\mu^{\mathrm{RT}}_{\mathrm{eff}} : \mu^{\mathrm{LT}}_{\mathrm{eff}}$ = 2.0, calculated using the magnetic moment of 2.83μ_B for the triplet Ni ion, is reasonably close to the experimentally observed range. The predicted effective magnetic moment of the RT structure in the presence of high-spin Fe and Ni ions equals 5.66μ_B, which is only 3% higher than that observed in Ref. 45 and 4%–7% higher than the values reported in Ref. 15. Therefore, the high-spin Ni represents a plausible alternative explanation of the magnetic properties of **1**. It means that Ni is not involved in the spin crossover process, but it is responsible for the augmented magnetic moment of the RT phase as compared to the pure high-spin

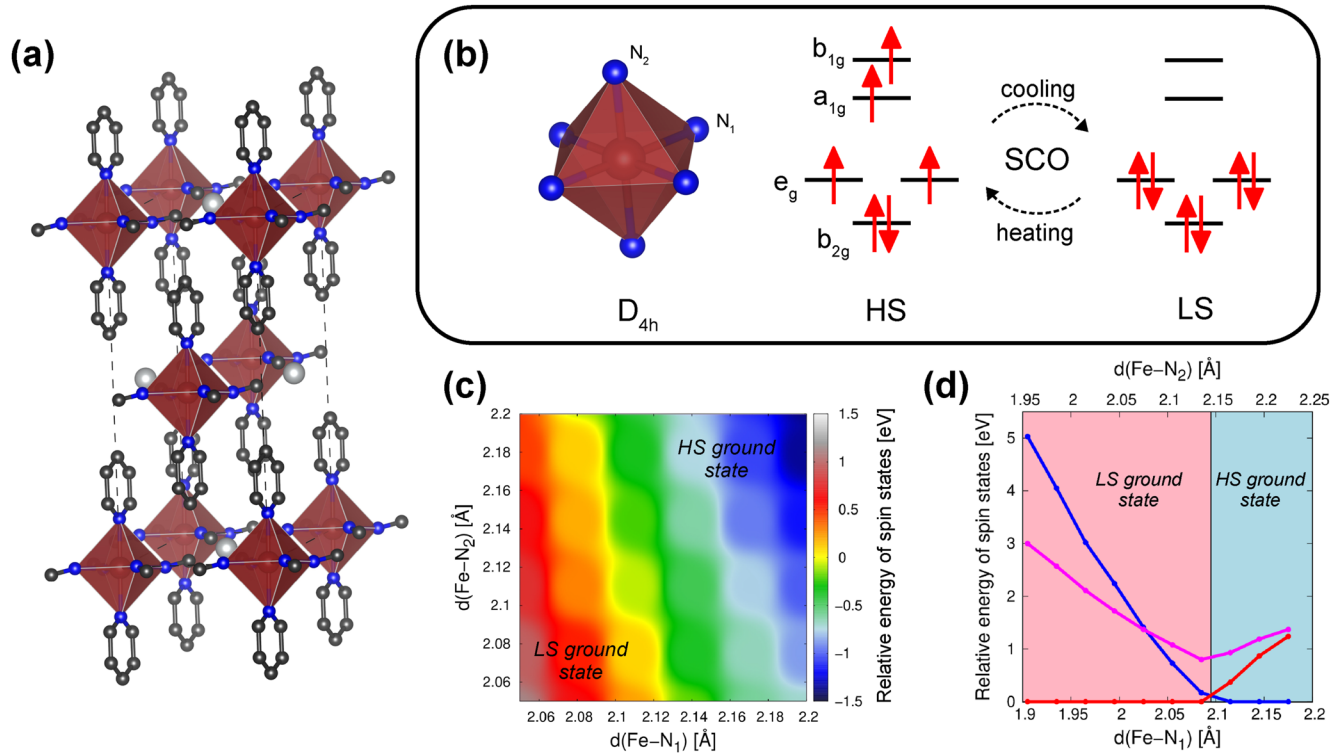

FIG. 1. (a) Crystal structure of **1**: the dark-red polyhedra correspond to the coordination spheres of Fe ions, the gray spheres correspond to Ni, the blue spheres represent N, the black spheres represent C, and the H atoms are not shown; (b) splitting diagram of Fe *d*-orbitals in the D_{4h} crystal field and spin-crossover transition for the d^6 configuration; (c) two-dimensional diagram of the relative energy between the high-spin and low-spin electronic states as a function of $d(Fe–N_1)$ and $d(Fe–N_2)$ distances within the Fe coordination sphere; (d) the energy of the states with different spins relative to the ground state as a function of $d(Fe–N_1)$ and $d(Fe–N_2)$: the blue line corresponds to $S = 2$ (HS), red to $S = 0$ (LS), and magenta to $S = 1$.

Fe (II) and a residual paramagnetism of the LT phase. Our calculations of the electronic structure of **1** support this hypothesis and yield high-spin ($S = 1$) configuration of Ni (II) ions in both RT and LT structures; see Table I.

Although compatible with the magnetic measurements, the high-spin ground state of the Ni atom in the presence of cyanide groups, usually referred to as strong-field ligands, might appear surprising. This result can be readily compared to similar solid compounds $Ni(CN)_2MX$ (M = Rb, Cs; X = Cl, Br) exhibiting low-spin of Ni (II) ions coordinated with cyanide ligands.[46] The splitting diagram of Ni *d*-states corresponds to square-planar geometry, and the splitting parameters Δ_{1-3} are given in Table I. The parameter Δ_3 corresponds to the splitting of the octahedral e_g manifold, and its value determines spin of the ground state of nickel. Although

TABLE I. Spin of the ground state, splitting parameters (in eV), and ^{57}Fe Mössbauer quadrupole splitting (in mm/s) calculated for open *d*-shells of Fe and Ni ions in system **1**.

	Fe		Ni	
	Room T	Low T	Room T	Low T
S	2	0	1	1
Δ_1	0.48	0.69	0.04	0.02
Δ_2	1.57	3.90	0.11	0.10
Δ_3	0.03	0.59	1.72	0.81
QS	3.62	1.65	⋯	⋯

TABLE II. Calculated energies (in eV) of *d*–*d* transitions for open *d*-shells of Fe and Ni ions in system **1**. Letters "A" and "E" in parentheses indicate if the state is non-degenerate or doubly degenerate, respectively.

Room T				Low T			
Fe		Ni		Fe		Ni	
Spin	Energy	Spin	Energy	Spin	Energy	Spin	Energy
2 (A)	0	1 (A)	0	0 (A)	0	1 (A)	0
2 (E)	0.48	1 (E)	0.22	1 (E)	2.58	1 (E)	0.13
0 (A)	1.01	0 (A)	0.72	0 (E)	3.67	1 (A)	0.59
1 (E)	1.26	1 (A)	0.92	1 (E)	3.75	1 (A)	0.80
1 (A)	1.68	1 (A)	1.72	1 (A)	3.79	1 (E)	0.84
1 (E)	1.85	1 (E)	1.79	1 (A)	3.92	0 (A)	1.44
2 (A)	2.05	0 (A)	1.93	2 (A)	4.05	0 (A)	1.87

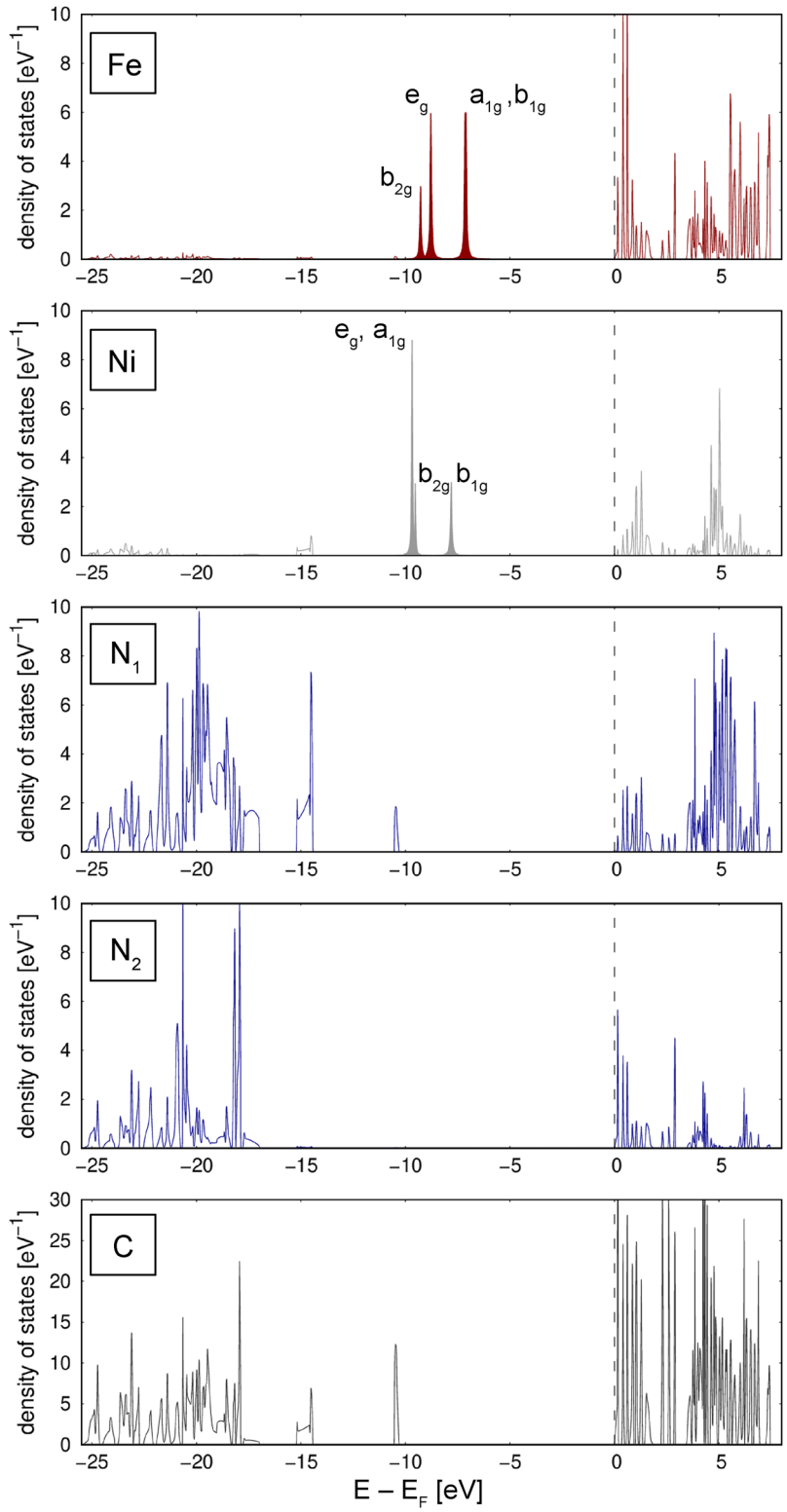

FIG. 2. Atomically projected densities of states of **1**. The filled peaks correspond to (partially) filled *d*-states of Fe and Ni. Note that some peaks correspond to *d*-levels of different symmetries lying close to each other, and are not resolved on the plot; hence, there are notations containing several irreducible representations.

the RT structure of **1** has the same geometry of the first coordination sphere of Ni as $Ni(CN)_2MX$, the calculated value of the Δ_3 splitting parameter in $Ni(CN)_2MX$ is 3.72 eV,[46] which is twice larger than that obtained in this work for the RT structure of **1** (Δ_3 = 1.72 eV; see Table I). Such a substantial difference in the splitting parameter is responsible for different spins of the ground state of the Ni ion in these two systems. Our analysis shows that the larger value of Δ_3 in $Ni(CN)_2MX$ is due to the higher resonance contribution expressed in Eq. (4), which corresponds to electron transfer from ligand orbitals to the *d*-shell of Ni. For $Ni(CN)_2MX$, the energy of electron transfer between the frontier orbitals of CN and Ni 3*d* orbitals is equal to 2.30 eV, while the same energy for the RT structure of **1** is 5.56 eV. The value of the Green function $\Re G^-$ entering Eq. (4) is inversely proportional to the energy of the electron transfer, which explains a larger splitting in $Ni(CN)_2MX$ as compared to structure **1**.

The density of states (DOS) for the RT and LT structures has a similar profile, and the atom-projected DOS at RT is shown in Fig. 2. The valence band of the *l*-subspace below the Fermi level has a frontier peak corresponding to CN groups, whereas the orbitals of pyridine nitrogen atoms (N_2) contribute to the deeper lying states. The local one-electron *d*-states of Fe and Ni are located in the bandgap of the *l*-system. Splitting of the Fe *d*-orbitals corresponds to irreducible representations of the D_{4h} group [see Fig. 1(b)], and the splitting parameters for the RT and LT structures are also collected in Table I. Parameters Δ_1 and Δ_3 correspond to the distortion of the ideal octahedron and are rather small compared to Δ_2 representing 10*Dq* parameter in octahedral complexes. The LT structure exhibits a much stronger splitting, which naturally leads to the low-spin ground state. The calculated difference in Δ_2 for the RT and LT structures can be attributed to a combination of the increase in the value of resonance integrals between the *d* orbitals of Fe and N and the decrease in the relative energy of N 2*p* and Fe 3*d* states. At the same time, the variation in the population of N atomic orbitals of the RT and LT structures is negligible and it does not contribute to the change in Δ_2.

The calculated spectra of the excited *d*–*d* states for the RT and LT structures are presented in Table II. In both cases, the energy difference between the ground state and the excited state with a different spin is high, $E_{HS} - E_{LS}$ = 4.05 eV for the LT structure and $E_{HS} - E_{LS}$ = −1.01 eV for the RT structure. This means that both structures are relatively far from the degeneracy point. We next investigate the behavior of the $E_{HS} - E_{LS}$ energy difference as a function of structural deformation accompanying spin-transition. To do that, we must first identify the relevant structural deformations. Raman spectroscopy of **1** shows[47] that when moving from the RT to LT structure, the change in frequencies corresponding to vibrations of CN and pyridine groups is very small, suggesting that the geometry of the ligands does not undergo a significant change during spin-transition. However, in the RT to LT transition, Fe–N bonds become shorter while Ni–C bonds increase in length, and SCO is accompanied by a shift of CN and pyridine groups as a whole. This conclusion is supported by XRD[48] and EXAFS[44] studies of **1** and similar structures where Ni is substituted by Pd and Pt. XRD experiments also demonstrate that the change in the unit cell volume is rather small (~3%) and preserves the symmetry of the compound. As we show below, this small contraction of the volume has little effect on the behavior of $E_{HS} - E_{LS}$. These careful considerations allow us to describe the deformation as a two-dimensional manifold with coordinates corresponding to $d(Fe–N_1)$ and $d(Fe–N_2)$ distances.

The values of $E_{HS} - E_{LS}$ as a function of these two distances are plotted in Fig. 1(c). The yellow boundary indicates the line of degeneracy between the HS and LS states, while the orange-red region corresponds to the stable LS state and the green-blue region corresponds to the stable HS state. Figure 1(c) shows that the dependence of the degeneracy line on the distance $Fe–N_1$ is rather sharp, and spin transition occurs in a narrow region of $d(Fe–N_1)$ = 2.08–2.12 Å. The dependence on $d(Fe–N_2)$ is weak in the intervals 2.05–2.08 and 2.12–2.18 Å and exhibits a step-like change in a narrow range $d(Fe–N_2)$ = 2.08–2.10 Å. The observed trend that the relative energy is more sensitive to $Fe–N_1$ separation is due to the fact that the N_1 2*p*–Fe 3*d* hopping is much stronger because of the frontier peak in the valence band attributed to the CN groups. A cut through the two-dimensional diagram in Fig. 1(c) is shown in Fig. 1(d), which looks similar to Tanabe–Sugano diagrams but is expressed as a function of the principal geometrical parameter describing SCO deformation. The degeneracy point is located at $d(Fe–N_1)$ = 2.085 Å, and for all $d(Fe–N_1) < 2.085$ Å, the ground state remains to be the LS state. The state with $S = 1$ (magenta) is never the ground state, but for

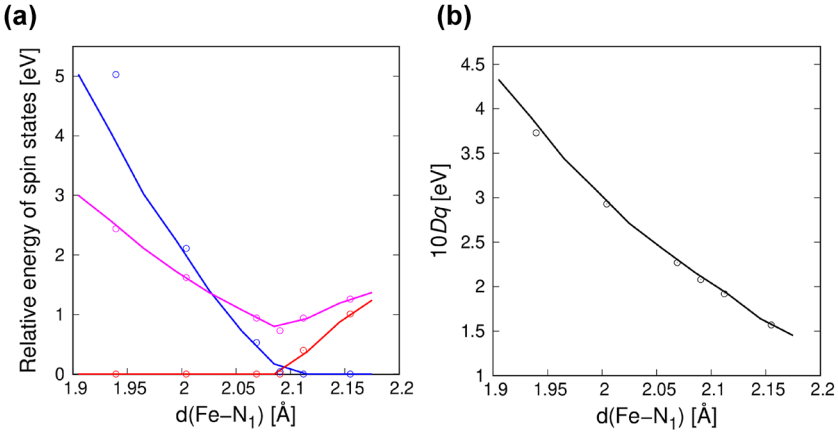

FIG. 3. Relative energies of the states with different spins (a) and splitting parameters Δ_2 (b) as functions of $d(Fe–N_1)$. The solid lines correspond to the deformation that does not change the volume of the unit cell, and the circles correspond to the case of uniform volume compression. The blue line corresponds to $S = 2$ (HS), red to $S = 0$ (LS), and magenta to $S = 1$.

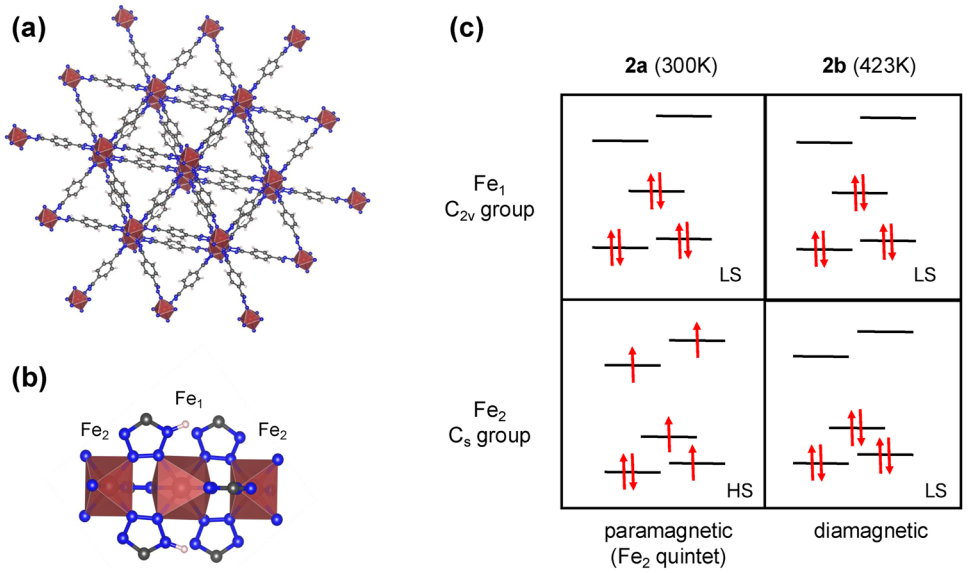

FIG. 4. (a) Crystal structure of 2. The color code is the same as in Fig. 1. (b) Fragment of the structure showing coordination spheres of Fe_1 and Fe_2 ions. (c) Splitting diagrams, local point groups, and spin-states of Fe_1 and Fe_2 ions for structures **2a** and **2b** corresponding to temperatures 300 and 423 K.

the LT structure, it lies lower in energy than the HS term $S = 2$ and, therefore, it is the lowest excited state.

Finally, we analyze how the variation of the unit cell volume affects the behavior of the relative energies of the HS and LS terms. We consider a deformation corresponding to the uniform compression of the volume, calculate the energies of the HS and LS states, and plot them as a function of the $d(Fe–N_1)$ distance [see Fig. 3(a)]. The relative energy follows the same trend for both deformations, and its values are very close in a wide range of $Fe–N_1$ separations, except for the vicinity of the LT structure. Here, the position of the degeneracy point remains almost the same. Figure 3(b) demonstrates that the values of the splitting parameter Δ_2, equivalent to $10Dq$, are also very close for both deformations. This implies that the only significant effect of the volume compression is contraction of the $Fe–N_1$ and $Fe–N_2$ distances and justifies neglecting ~3% compression of the unit cell volume (as observed for **1** in experiment) in the two-dimensional manifold of the full potential energy surface shown in Fig. 1(c).

A recent study[27] reported a SCO-MOF $Fe_2(H_{0.67}bdt)_3$ (**2**) exhibiting unusual spin crossover when heated above the room temperature. This system contains two types of iron (II) ions, Fe_1 and Fe_2, each surrounded by six nitrogen atoms of tetrazole fragments as illustrated in Figs. 4(a) and 4(b). Tetrazole fragments act as bidentate ligands, one nitrogen atom of which coordinates Fe_1 ions while the other chelates Fe_2 ions, thus forming bridges between the two iron atoms. At room temperature, system **2** is paramagnetic ($\chi_m T = 3.18$ cm^3 K/mol) and has the crystal structure **2a** determined experimentally by XRD.[27] It contains water molecules in pores yielding the overall composition $Fe_2(H_{0.67}bdt)_3 \cdot 9H_2O$. In this structure, Fe_1 is found to have low-spin ($S = 0$), while Fe_2 has high-spin ($S = 2$) and is responsible for paramagnetism of **2a**. Once heated above 300 K, the value of $\chi_m T$ begins to fall with temperature, which is unusual as typically the magnetic moment is increased upon heating in an SCO system. This happens due to the loss of water absorbed in the pores and consequent adjustment of the crystal geometry that involves the change of the coordination spheres of the iron ions. At about 423 K, the system reaches diamagnetic state **2b** with the composition $Fe_2(H_{0.67}bdt)_3 \cdot 2H_2O$. The $Fe_1–N$ and $Fe_2–N$ interatomic distances experimentally determined in structures **2a** and **2b** are collected in Table III. The experimental study Ref. 27 also identified an additional structure of system **2** with composition $Fe_2(H_{0.67}bdt)_3 \cdot 4H_2O$ corresponding to 340–345 K with an intermediate value of the magnetic susceptibility $\chi_m T = 1.89$ cm^3 K/mol. However, the structure of this compound was found to be substantially disordered[49] and therefore not considered in this work.

We investigate the electronic structure of **2a** and **2b** using the pEHCF method (Fig. 5). Water molecules existing in the pores are not coordinated to the iron ions and affect the magnetic properties of system **2** indirectly through the structural deformations associated with the loss of water. Therefore, in our analysis, the water molecules are omitted. The pEHCF calculations show that structure **2a** has low-spin Fe_1 ion and high-spin Fe_2 ion in the ground state, while **2b** contains both ions in the low-spin configuration [Fig. 4(c)]. This

TABLE III. Fe–N separation (in Å), spin of the ground state, splitting parameters (in eV), and ^{57}Fe Mössbauer quadrupole splitting (in mm/s) calculated for open *d*-shells of Fe_1 and Fe_2 ions in system **2** for two different structures **2a** and **2b** corresponding to temperatures of 300 and 423 K.

	Fe_1		Fe_2	
	2a	**2b**	**2a**	**2b**
d(Fe–N)	1.97	1.91	2.18	1.97
S	0 (LS)	0 (LS)	2 (HS)	0 (LS)
Δ_1	0.81	0.12	0.14	0.14
Δ_2	0.12	0.07	0.02	0.05
Δ_3	3.45	5.75	1.59	3.85
Δ_4	1.85	0.93	0.06	1.91
QS	0.43	0.27	3.02	0.47

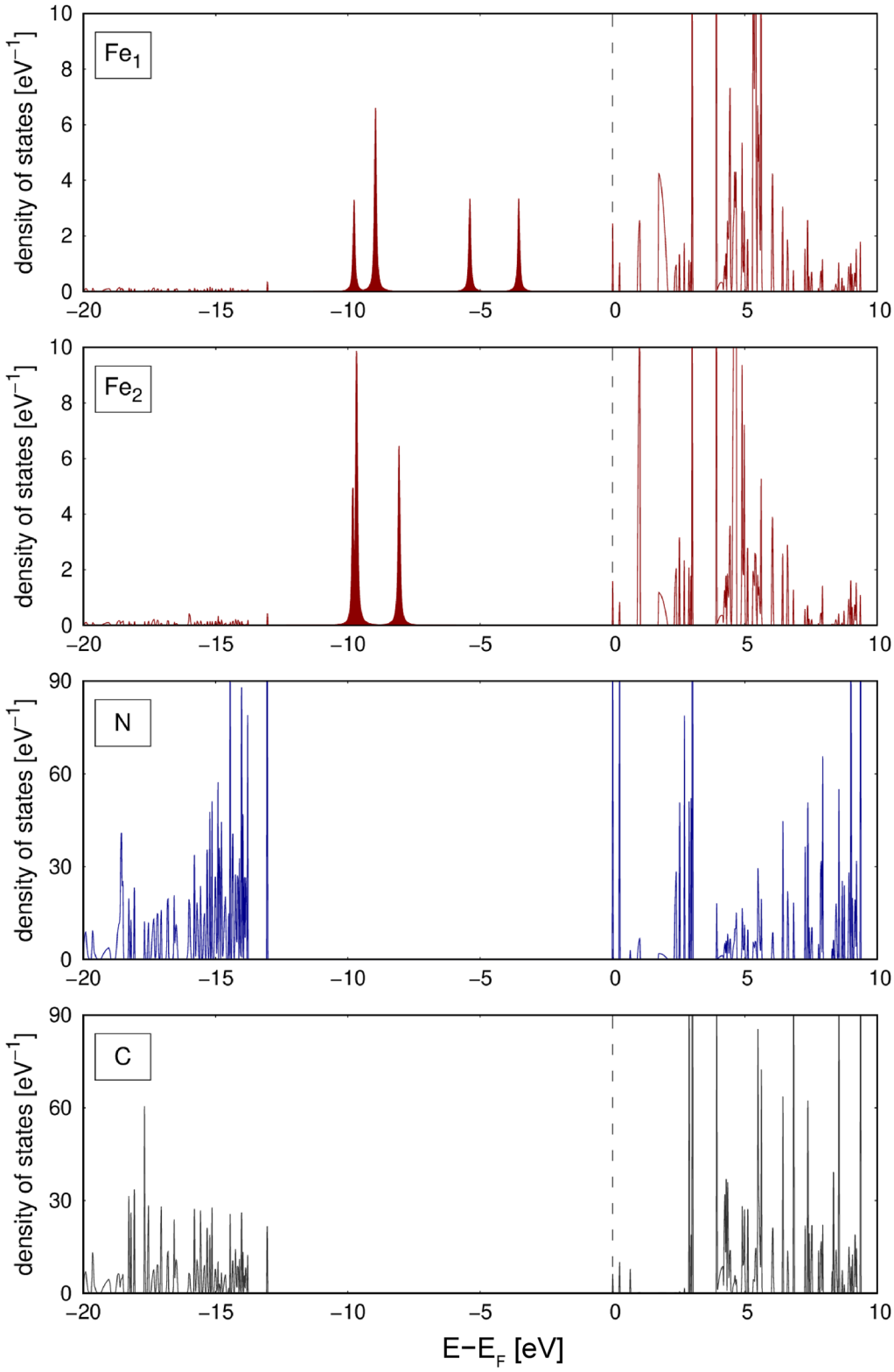

FIG. 5. Atomically projected densities of states of system **2a**.

result is in complete agreement with experimental measurements and DFT+U calculations performed previously.[27]

The pEHCF calculated splitting parameters of the one-electron d-states are collected in Table III. From these values, it is evident that the degeneracy within t_{2g} and e_g manifolds is completely lifted, the energy separation between these manifolds is given by Δ_3, and the splitting within the manifolds is characterized by Δ_{1-2} and Δ_4. The six nitrogen atoms surrounding the Fe_1 ion can be divided into three groups according to their values of the partial atomic charges. As a result, the total symmetry of Fe_1 crystal field is lowered to C_{2v}. An analogous picture is observed for the Fe_2 ion with the local symmetry of charge distribution corresponding to C_s group. Such asymmetry in the population of nitrogen atoms is caused by two geometrical factors: distortions of the coordination spheres of iron ions and the fact that only two of six tetrazolate rings in the unit cell are protonated. This makes the ligands in system **2** non-identical.

IV. COMPUTATIONAL DETAILS

The crystalline structures of systems **1** and **2** were taken from Refs. 13 and 27 as deposited in the CSD database.[50] Calculations were performed in the software implementing pEHCF and reported in our previous work (Ref. 39). The resonance integrals entering Eq. (4) are calculated as

$$\beta_{\mu a} = \beta^{ML}(I_\mu + I_a)S_{\mu a}, \quad \mu \in M, \quad a \in L, \tag{8}$$

where $S_{\mu a}$ is the overlap integral between orbitals μ and a that depends on the distance between atoms M and L, I_μ and I_a are corresponding ionization potentials, and β^{ML} are scaling parameters for a given pair of atoms M and L.[42] These scaling parameters were originally fitted for a series of iron-containing molecular complexes,[51] and in this work, we use these values without any additional reparameterization. The values of the resonance scaling parameters are $\beta^{Fe-N} = 1.505$, $\beta^{Fe-C} = 1.263$, $\beta^{Ni-N} = 1.535$, $\beta^{Ni-C} = 0.857$, while for all other pairs of atoms, $\beta^{ML} = 1$, as their contribution is minor due to the exponential decay of the overlap integrals with the interatomic separation.

The band structure and density of states of the l-subsystems were calculated using the periodic Hartree–Fock method in the basis of local atomic orbitals with the Ewald summation for the long-range Coulomb interactions. $(5 \times 5 \times 5)$ Monkhorst–Pack k-mesh was used for **1**, and $(3 \times 3 \times 3)$ Monkhorst–Pack k-mesh was used for system **2**. Linear CI equations for the d-shells were solved in the basis of the Young tableaux as implemented in the CRYSTAL FORT library.[52] The two-dimensional graph shown in Fig. 1(c) was obtained by calculating the relative energy of HS and LS states for each point of a discrete 11×11 mesh and interpolating the data.

V. CONCLUSIONS

The pEHCF method has been used to study the electronic structure and energetics of HS and LS states of spin crossover MOFs containing strongly correlated d-shells of iron (II) ions. For the Hofmann-type framework, $Fe(pyridine)_2Ni(CN)_4$ SCO-MOF, we have identified a two-dimensional manifold of structural parameters describing deformations accompanying spin transition and calculated the energy of HS and LS states in this manifold. We have also found a line of degeneracy of the spin states and described its dependence on the interatomic distances $d(Fe–N_1)$ and $d(Fe–N_2)$. Our results show that the Ni ion of system **1** exists in high spin configuration, which explains the non-vanishing magnetic moment observed at low temperatures.

The electronic structure of two configurations of $Fe_2(H_{0.67}bdt)_3$ SCO-MOF was also studied by the pEHCF method to elucidate the changes in the d-shells of iron ions upon spin transition. Our results show that Fe_2 ions undergo a transition from quintet $(S = 2)$ to singlet $(S = 0)$ state in the range of temperature 300–423 K. At the same time, Fe_1 ions have the low-spin ground state in both structures corresponding to 300 and 423 K.

Frequently, SCO studies have been focusing on macroscopic characteristics of this process, such as temperature dependence of magnetization or relative fraction of ions with high spin and low spin electronic configurations. These macroscopic features of SCO can be accurately described using classical methods of thermodynamics and statistical physics, which include the phenomenological Slichter–Drickamer model,[53] the Ising-like model,[54–56] and elastic[57–60] models, among many others.[61,62] Although these methods provide a detailed description of SCO for a large ensemble of spin centers, they are not capable of capturing the intricate changes in the electronic structure accompanying a transition. The missing atomic-scale insight, as provided by this study, is critical for deepening our understanding of SCO as it relates the change of the ground state of an individual TM ion with structure deformations and provides a quantitative estimate of the energy parameters used in statistical macroscopic models.

ACKNOWLEDGMENTS

E.B. acknowledges a Royal Society Wolfson Fellowship and EPSRC Programme Grant "Metal Atoms on Surfaces and Interfaces (MASI) for Sustainable Future" (Grant No. EP/V000055/1) for financial support. A.T. was supported by the Ministry of Science and Higher Education of the Russian Federation.

AUTHOR DECLARATIONS

Conflict of Interest

The authors have no conflicts to disclose.

Author Contributions

I. Popov: Conceptualization (equal); Formal analysis (equal); Investigation (lead); Writing – review & editing (equal). **A. Tchougréeff**: Conceptualization (equal); Formal analysis (equal); Writing – review & editing (equal). **E. Besley**: Conceptualization (equal); Formal analysis (equal); Project administration (lead); Writing – review & editing (equal).

DATA AVAILABILITY

The data that support the findings of this study are available from the corresponding author upon reasonable request.

REFERENCES

[1] G. Molnár, S. Rat, L. Salmon, W. Nicolazzi, and A. Bousseksou, "Spin crossover nanomaterials: From fundamental concepts to devices," Adv. Mater. **30**, 17003862 (2017).

[2] *Spin-Crossover Materials*, edited by M. A. Halcrow (Wiley, 2013).

[3] S. M. Neville, G. J. Halder, K. W. Chapman, M. B. Duriska, P. D. Southon, J. D. Cashion, J.-F. Létard, B. Moubaraki, K. S. Murray, and C. J. Kepert, "Single-crystal to single-crystal structural transformation and photomagnetic properties of a porous iron(II) spin-crossover framework," J. Am. Chem. Soc. **130**, 2869–2876 (2008).

[4] S. M. Neville, G. J. Halder, K. W. Chapman, M. B. Duriska, B. Moubaraki, K. S. Murray, and C. J. Kepert, "Guest tunable structure and spin crossover properties in a nanoporous coordination framework material," J. Am. Chem. Soc. **131**, 12106–12108 (2009).

[5] K. Otsubo, T. Haraguchi, and H. Kitagawa, "Nanoscale crystalline architectures of Hofmann-type metal–organic frameworks," Coord. Chem. Rev. **346**, 123–138 (2017).

[6] G. J. Halder, C. J. Kepert, B. Moubaraki, K. S. Murray, and J. D. Cashion, "Guest-dependent spin crossover in a nanoporous molecular framework material," Science **298**, 1762–1765 (2002).

[7] G. J. Halder, K. W. Chapman, S. M. Neville, B. Moubaraki, K. S. Murray, J.-F. Létard, and C. J. Kepert, "Elucidating the mechanism of a two-step spin transition in a nanoporous metal–organic framework," J. Am. Chem. Soc. **130**, 17552–17562 (2008).

[8] I. Strauss, A. Mundstock, M. Treger, K. Lange, S. Hwang, C. Chmelik, P. Rusch, N. C. Bigall, T. Pichler, H. Shiozawa, and J. Caro, "Metal–organic framework Co-MOF-74-based host–guest composites for resistive gas sensing," ACS Appl. Mater. Interfaces **11**, 14175–14181 (2019).

[9] H. Y. Li, S. N. Zhao, S. Q. Zang, and J. Li, "Functional metal–organic frameworks as effective sensors of gases and volatile compounds," Chem. Soc. Rev. **49**, 6364–6401 (2020).

[10] Y. Zheng, J. Yong, Z. Zhu, J. Chen, Z. Song, and J. Gao, "Spin crossover in metal–organic framework for improved separation of C_2H_2/CH_4 at room temperature," J. Solid State Chem. **304**, 122554 (2021).

[11] B. Brachňaková, J. Moncol', J. Pavlik, I. Šalitroš, S. Bonhommeau, F. J. Valverde-Muñoz, L. Salmon, G. Molnár, L. Routaboul, and A. Bousseksou, "Spin crossover metal–organic frameworks with inserted photoactive guests: On the quest to control the spin state by photoisomerization," Dalton Trans. **50**, 8877–8888 (2021).

[12] J.-P. Xue, Y. Hu, B. Zhao, Z.-K. Liu, J. Xie, Z.-S. Yao, and J. Tao, "A spin-crossover framework endowed with pore-adjustable behavior by slow structural dynamics," Nat. Commun. **13**, 3510 (2022).

[13] T. Kitazawa, Y. Gomi, M. Takahashi, M. Takeda, M. Enomoto, A. Miyazaki, and T. Enoki, "Spin-crossover behaviour of the coordination polymer $Fe^{II}(C_5H_5N)_2Ni^{II}(CN)_4$," J. Mater. Chem. **6**, 119 (1996).

[14] T. Wang, Y. Wu, Y. Han, P. Xu, Y. Pang, X. Feng, H. Yang, W. Ji, and T. Cheng, "Hofmann-type metal–organic framework nanosheets for oxygen evolution," ACS Appl. Nano Mater. **4**, 14161–14168 (2021).

[15] Y. Yang, X. Shen, H. Zhou, L. Lang, G. Zhu, and Z. Ji, "Controlled synthesis of $[Fe(pyridine)_2Ni(CN)_4]$ nanostructures and their shape-dependent spin-crossover properties," J. Magn. Magn. Mater. **496**, 165938 (2020).

[16] Z.-P. Ni, J.-L. Liu, M. N. Hoque, W. Liu, J.-Y. Li, Y.-C. Chen, and M.-L. Tong, "Recent advances in guest effects on spin-crossover behavior in Hofmann-type metal-organic frameworks," Coord. Chem. Rev. **335**, 28–43 (2017).

[17] M. J. Murphy, K. A. Zenere, F. Ragon, P. D. Southon, C. J. Kepert, and S. M. Neville, "Guest programmable multistep spin crossover in a porous 2-D Hofmann-type material," J. Am. Chem. Soc. **139**, 1330–1335 (2017).

[18] N. F. Sciortino, K. R. Scherl-Gruenwald, G. Chastanet, G. J. Halder, K. W. Chapman, J. Létard, and C. J. Kepert, "Hysteretic three-step spin crossover in a thermo- and photochromic 3D pillared Hofmann-type metal–organic framework," Angew. Chem., Int. Ed. **51**, 10154–10158 (2012).

[19] T. Kitazawa, M. Eguchi, and M. Takeda, "Crystal structures of two-dimensional coordination polymer $Fe(Methylpyridine)_2Ni(CN)_4$," Mol. Cryst. Liq. Cryst. Sci. Technol., Sect. A **341**, 527–532 (2000).

[20] T. Kitazawa, T. Kishida, T. Kawasaki, and M. Takahashi, "Spin crossover behaviour in hofmann-like coordination polymer $Fe(py)_2[Pd(CN)_4]$ with ^{57}Fe mössbauer spectra," Hyperfine Interact. **238**, 65 (2017).

[21] V. Martínez, A. B. Gaspar, M. C. Muñoz, G. V. Bukin, G. Levchenko, and J. A. Real, "Synthesis and characterisation of a new series of bistable iron(II) spin-crossover 2D metal–organic frameworks," Chem. - Eur. J. **15**, 10960–10971 (2009).

[22] G. Agustí, M. C. Muñoz, A. B. Gaspar, and J. A. Real, "Spin-crossover behavior in cyanide-bridged iron(II) - gold(I) bimetallic 2D Hofmann-like metal organic frameworks," Inorg. Chem. **47**, 2552–2561 (2008).

[23] M. C. Muñoz, A. B. Gaspar, A. Galet, and J. A. Real, "Spin-crossover behavior in cyanide-bridged iron(II) - silver(I) bimetallic 2D Hofmann-like metal organic frameworks," Inorg. Chem. **46**, 8182–8192 (2007).

[24] J. A. Rodríguez-Velamazán, K. Kitase, E. Palacios, M. Castro, Á. Fernández-Blanco, R. Burriel, and T. Kitazawa, "Structural insights into the two-step spin-crossover compound $Fe(3,4\text{-dimethyl-pyridine})_2[Ag(CN)_2]_2$," Crystals **9**, 316 (2019).

[25] C. H. Pham and F. Paesani, "Spin crossover in the $\{Fe(pz)[Pt(CN)_4]\}$ metal–organic framework upon pyrazine adsorption," J. Phys. Chem. Lett. **7**, 4022–4026 (2016).

[26] M. Grzywa, R. Röß-Ohlenroth, C. Muschielok, H. Oberhofer, A. Błachowski, J. Żukrowski, D. Vieweg, H.-A. K. von Nidda, and D. Volkmer, "Cooperative large-hysteresis spin-crossover transition in the iron(II) triazolate $[Fe(ta)_2]$ metal–organic framework," Inorg. Chem. **59**, 10501–10511 (2020).

[27] A. Martinez-Martinez, E. Resines-Urien, L. Piñeiro-López, A. Fernández-Blanco, A. Lorenzo Mariano, J. Albalad, D. Maspoch, R. Poloni, J. A. Rodríguez-Velamazán, E. C. Sañudo, E. Burzurí, and J. Sánchez Costa, "Spin crossover-assisted modulation of electron transport in a single-crystal 3D metal–organic framework," Chem. Mater. **35**, 6012–6023 (2023).

[28] Y. Tanabe and S. Sugano, "On the absorption spectra of complex ions. I," J. Phys. Soc. Jpn. **9**, 753–766 (1954).

[29] Q. M. Phung, M. Feldt, J. N. Harvey, and K. Pierloot, "Toward highly accurate spin state energetics in first-row transition metal complexes: A combined CASPT2/CC approach," J. Chem. Theory Comput. **14**, 2446–2455 (2018).

[30] L. M. Lawson Daku, F. Aquilante, T. W. Robinson, and A. Hauser, "Accurate spin-state energetics of transition metal complexes. 1. CCSD(T), CASPT2, and DFT Study of $[M(NCH)_6]^{2+}$ (M = Fe, Co)," J. Chem. Theory Comput. **8**, 4216–4231 (2012).

[31] B. M. Flöser, Y. Guo, C. Riplinger, F. Tuczek, and F. Neese, "Detailed pair natural orbital-based coupled cluster studies of spin crossover energetics," J. Chem. Theory Comput. **16**, 2224–2235 (2020).

[32] S. Vancoillie, H. Zhao, M. Radoń, and K. Pierloot, "Performance of CASPT2 and dft for relative spin-state energetics of heme models," J. Chem. Theory Comput. **6**, 576–582 (2010).

[33] B. A. Finney, S. R. Chowdhury, C. Kirkvold, and B. Vlaisavljevich, "CASPT2 molecular geometries of Fe(II) spin-crossover complexes," Phys. Chem. Chem. Phys. **24**, 1390–1398 (2022).

[34] M. C. Demuth, K. N. Le, M. Sciprint, and C. H. Hendon, "Ligand-engineered spin crossover in Fe(II)-based molecular and metal–organic framework systems," J. Phys. Chem. C **127**, 2735–2740 (2023).

[35] V. Vennelakanti, M. G. Taylor, A. Nandy, C. Duan, and H. J. Kulik, "Assessing the performance of approximate density functional theory on 95 experimentally characterized Fe(II) spin crossover complexes," J. Chem. Phys. **159**, 024120 (2023).

[36] D. Nazarian, J. S. Camp, Y. G. Chung, R. Q. Snurr, and D. S. Sholl, "Large-scale refinement of metal–organic framework structures using density functional theory," Chem. Mater. **29**, 2521–2528 (2016).

[37] A. L. Tchougréeff, A. V. Soudackov, J. van Leusen, P. Kögerler, K.-D. Becker, and R. Dronskowski, "Effective hamiltonian crystal field: Present status and applications to iron compounds," Int. J. Quantum Chem. **116**, 282–294 (2015).

[38] I. Popov, E. Plekhanov, A. Tchougréeff, and E. Besley, "Effective Hamiltonian of crystal field method for periodic systems containing transition metals," Mol. Phys. **121**, e2106905 (2023).

[39] I. Popov, D. Raenko, A. Tchougréeff, and E. Besley, "Electronic structure and d–d spectrum of metal–organic frameworks with transition-metal ions," J. Phys. Chem. C **127**, 21749–21757 (2023).

[40] W. Harrison, *Electronic Structures and the Properties of Solids: The Physics of the Chemical Bond* (Freeman Company, San Francisco, 1980).
[41] D. W. Clack, N. S. Hush, and J. R. Yandle, "All-valence electron CNDO calculations on transition metal complexes," J. Chem. Phys. **57**, 3503–3510 (1972).
[42] A. V. Soudackov, A. L. Tchougréeff, and I. A. Misurkin, "Electronic structure and optical spectra of transition metal complexes by the effective Hamiltonian method," Theor. Chim. Acta **83**, 389–416 (1992).
[43] P. Löwdin, "Partitioning technique, perturbation theory, and rational approximations," Int. J. Quantum Chem. **21**, 69–92 (1982).
[44] J. Okabayashi, S. Ueno, Y. Wakisaka, and T. Kitazawa, "Temperature-dependent EXAFS study for spin crossover complex: $Fe(pyridine)_2Ni(CN)_4$," Inorg. Chim. Acta **426**, 142–145 (2015).
[45] K. Hosoya, T. Kitazawa, M. Takahashi, M. Takeda, J.-F. Meunier, G. Molnár, and A. Bousseksou, "Unexpected isotope effect on the spin transition of the coordination polymer $Fe(C_5H_5N)_2[Ni(CN)_4]$," Phys. Chem. Chem. Phys. **5**, 1682–1688 (2003).
[46] X. Liu, M. Speldrich, P. Kögerler, R. Dronskowski, and A. L. Tchougréeff, "Synthesis, characterization, and quantum-chemical studies of $Ni(CN)_2MX$ (M = Rb, Cs; X = Cl, Br)," Inorg. Chem. **49**, 7414–7423 (2010).
[47] G. Molnár, V. Niel, A. B. Gaspar, J.-A. Real, A. Zwick, A. Bousseksou, and J. J. McGarvey, "Vibrational spectroscopy of cyanide-bridged, iron(II) spin-crossover coordination polymers: Estimation of vibrational contributions to the entropy change associated with the spin transition," J. Phys. Chem. B **106**, 9701–9707 (2002).
[48] S. Sakaida, K. Otsubo, M. Maesato, and H. Kitagawa, "Crystal size effect on the spin-crossover behavior of $\{Fe(py)_2[Pt(CN)_4]\}$ (py = pyridine) monitored by Raman spectroscopy," Inorg. Chem. **59**, 16819–16823 (2020).
[49] A. Martinez-Martinez, J. Albalad, E. Resines-Urien, E. C. Sañudo, A. L. Mariano, O. Fabelo, J. A. Rodríguez-Velamazán, R. Poloni, D. Maspoch, and J. S. Costa, "Decoding framework dynamics in a spin crossover flexible metal–organic framework," Small **21**, 2411201 (2025).
[50] F. H. Allen, S. Bellard, M. D. Brice, B. A. Cartwright, A. Doubleday, H. Higgs, T. Hummelink, B. G. Hummelink-Peters, O. Kennard, W. D. S. Motherwell, J. R. Rodgers, and D. G. Watson, "The Cambridge crystallographic data centre: Computer-based search, retrieval, analysis and display of information," Acta Crystallogr., Sect. B **35**, 2331–2339 (1979).
[51] A. Soudackov, A. L. Tchougréeff, and I. A. Misurkin, "Calculations on electronic structure of octahedral hexaqua and hexammino complexes of first row transition metals by the effective Hamiltonian method," Russ. J. Phys. Chem. **68**, 1135 (1994).
[52] A. L. Tchougréeff, "Cartesius fort - object Fortran library for chemistry and materials science," in *Computational Science and its Applications – ICCSA 2019*, edited by S. Misra, O. Gervasi, B. Murgante, E. Stankova, V. Korkhov, C. Torre, A. M. A. Rocha, D. Taniar, B. O. Apduhan, and E. Tarantino (Springer International Publishing, Cham, 2019), pp. 639–651.
[53] C. P. Slichter and H. G. Drickamer, "Pressure-induced electronic changes in compounds of iron," J. Chem. Phys. **56**, 2142–2160 (1972).
[54] J. Wajnflasz and R. Pick, "Transitions 'low spin'-'high spin' dans les complexes de Fe^{2+}," J. Phys. Colloq. **32**, C1–91–C1–92 (1971).
[55] K. Boukheddaden, I. Shteto, B. Hôo, and F. Varret, "Dynamical model for spin-crossover solids. I. Relaxation effects in the mean-field approach," Phys. Rev. B **62**, 14796–14805 (2000).
[56] J. Pavlik and J. Linares, "Microscopic models of spin crossover," C. R. Chim. **21**, 1170–1178 (2018).
[57] M. Nishino, K. Boukheddaden, Y. Konishi, and S. Miyashita, "Simple two-dimensional model for the elastic origin of cooperativity among spin states of spin-crossover complexes," Phys. Rev. Lett. **98**, 247203 (2007).
[58] Y. Konishi, H. Tokoro, M. Nishino, and S. Miyashita, "Monte Carlo simulation of pressure-induced phase transitions in spin-crossover materials," Phys. Rev. Lett. **100**, 067206 (2008).
[59] C. Enachescu, L. Stoleriu, A. Stancu, and A. Hauser, "Model for elastic relaxation phenomena in finite 2D hexagonal molecular lattices," Phys. Rev. Lett. **102**, 257204 (2009).
[60] A.-I. Popa, L. Stoleriu, and C. Enachescu, "Tutorial on the elastic theory of spin crossover materials," J. Appl. Phys. **129**, 131101 (2021).
[61] A. L. Tchougréeff and M. B. Darkhovskii, "Lattice relaxation and order in the low-spin to high-spin transitions in molecular crystals," Int. J. Quantum Chem. **57**, 903–912 (1996).
[62] J. Cirera, V. Babin, and F. Paesani, "Theoretical modeling of spin crossover in metal–organic frameworks: $[Fe(pz)_2Pt(CN)_4]$ as a case study," Inorg. Chem. **53**, 11020–11028 (2014).